LA-UR-15-20217 (Accepted Manuscript)

Internal sub-sonic burning during an explosion viewed via dynamic X-ray radiography

Henson, Bryan Fayne
Smilowitz, Laura Beth
Oschwald, David M.

To be published in: Applied Physics Letters

DOI to publisher's version: 10.1063/1.5004424

Permalink to record: http://permalink.lanl.gov/object/view?what=info:lanl-repo/lareport/LA-UR-15-20217

Internal Sub-Sonic Burning During an Explosion Viewed Via Dynamic X-Ray Radiography

L. Smilowitz, B. F. Henson, D. Oschwald, N. Suvorova, and D. Remelius

Los Alamos National Lab

Los Alamos, NM 87545

USA

PACS numbers: 82.33.Vx; 82.30.Lp; 47.70.Pq

ABSTRACT

We observe internal convective and conductive burn front propagation and solid consumption subsequent to thermal ignition for plastic bonded formulations of the solid organic secondary explosives octahydro-1,3,5,7-tetranitro-1,3,5,7-tetrazocine (HMX) and 1,3,5-triamino-2,4,6-trinitrobenzene (TATB). This work describes x-ray radiographic diagnostics enabling the study of solid density in a fully encased explosive during internal burning subsequent to ignition. The result of this study is the ability to directly observe and measure rates of energy release during a thermal explosion.

This manuscript was accepted by Appl. Phys. Lett. Click here to see the version of record.

The rate of chemical energy release in a thermal explosion has been the topic of considerable research for many years.[1] The release of energy in materials such as the HMX based plastic bonded explosives PBX 9501, PBXN-9 and TATB based PBX 9502 undergoing super-sonic detonation can be fairly well modelled. However, the response of these same materials subsequent to heating when encased and under confinement, resulting in thermal ignition and initial sub-sonic combustion propagation are relatively poorly understood.[1] There has been significant work over the past several years to measure the linear combustion rate as a function of pressure for these materials,[2-7] however there has been little data with which to associate these observations with processes that begin with ignition within the explosive. In previous work utilizing proton[8, 9] and flash x-ray[10, 11] radiography we have shown the utility of such internal observations to understanding phenomena both during heating to ignition and subsequent internal burning. In a recent letter we also presented preliminary results from a new laboratory scale dynamic x-ray radiographic experiment where we demonstrated the ability to image the evolution of internal solid density as a function of thermal decomposition and material transport due to heating prior to ignition[12] and propagation post-ignition.[12] In this letter we present initial results from the post-ignition application of this radiography, again to image the evolution of material density, but in this regime due to the conversion of solid to gas during internal combustion. Results showing multiple views of the evolution of solid density will be presented. Future work aimed at diagnosing and manipulating the rate of combustion in different formulations will be described.

This manuscript was accepted by Appl. Phys. Lett. Click here to see the version of record.

In the experiments described here, 6g cylinders of the energetic material, ½" diameter by 1" long, are encased in an aluminum sleeve and heated radially from outside the aluminum. The Al case is either constructed of two parts, joined at the midplane bisecting the cylinder into two half cylinders, or of a single cylinder of full length. Details of this radial thermal explosion geometry are presented in previous publications.[8, 13, 14] The technique for dynamic x-ray radiography of the post-ignition combustion regime utilizes either a modified medical x-ray source operating at 90 kVp with a 2 ms pulse duration or a continuous source also operating at 90 kVp. The 90 kVp peak x-ray energy is found to provide the optimal combination of x-ray flux for penetrating the ½" of energetic material and the ¼" of aluminum encasing it, while still providing adequate sensitivity to observe changes in solid density. The x-ray transmission was converted to a light image using a thallium doped structured CsI scintillator imaged by a scientific grade high speed video camera. Image times are determined relative to internal thermal signals which preceed ignition. The side on and radial viewing axes are illustrated using images of the cylindrical case in Fig. 1

When explosives such as HMX or TATB are heated to temperatures above their critical temperature, they will begin undergoing exothermic chemistry leading to ignition.[12] Ignition is the transition from thermal decomposition in the solid to conductive and convective combustion as the dominant mechanism of energy release. It divides the regimes of heating in place (Eulerian regime) and burn front propagation (Lagrangian regime). Experimentally we observe ignition as significant transients in internal thermocouple signals and Si and InGaAs photodiode intensity sampled by fiber optics from near the ignition location.[9] The full mechanism likely involves the ignition

of first conductive burning of the solid near the initial ignition location, possibly followed by convective propagation of surface ignition through the gas phase, igniting solid consumption by conductive regression from the local surface[9] The elucidation of this full mechanism will be the focus of future work utilizing these techniques. Ignition is followed promptly by the propagation of burning, as imaged by the x-ray radiography.

This is illustrated in Fig. 2, where a PBX 9501 sample is viewed down the cylinder axis. PBX 9501 is a plastic bonded explosive composed of 95% HMX and 2.5% estane mixed with 2.5% nitroplasticizer (BDNPA/F). Three x-ray images of direct, normalized transmission are shown on the left, and the transmission integrated horizontally through the region of increased transmission with 1 mm vertical resolution is shown on the right, with frame time relative to triggering noted in the figure. In all x-ray images shown here we use lighter grey to white to indicate higher transmission (lower density) and darker grey to black lower transmission. The interframe time is 10 μs. The solid black lines are guides to the eye based on preliminary modeling[15]. The experiments involving HMX and shown in Figs 2-4 were triggered using the slowly rising signal from an InGaAs IR diode coupled to a fiber optic embedded in the sample near the center of the cylinder, as described above. This allows the source and detection to be triggered prior to ignition to observe the transition between the two regimes. We observe three static frames prior to ignition, ignition defined as the beginning of propagation at t = 20 μs. The static, high transmission feature observed prior to ignition is the volume created by solid thermal decomposition established in PBX 9501 prior to ignition and previously reported.[12] The propagation of density loss is then observed as the expanding edge of the region of transmission increase, followed by a rising total transmission increase as a function of

This manuscript was accepted by Appl. Phys. Lett. Click here to see the version of record.

time. These observations are consistent with those made using proton radiography,[9] the interpretation being that the propagation of transmission increase indicates the propagation of burning by convection in the gas phase, igniting the solid surface. The overall transmission increase with time inside the edges is then a measure of solid consumption and conversion to gas phase products by conductive regression of the surface. A three point velocity obtained from the edge position as a function of frame time from 20, 30 and 40 μs is 164 m/s, in excellent agreement with 166 m/s radial velocity measured by proton radiography.[9] It is this relatively high subsonic combustion rate that leads to our interpretation of convective burning as the mechanism of propagation in HMX based formulations under these conditions of heating, confinement and ignition.[2,3] We show data from a second HMX formulation, PBXN-9, in Fig. 3. PBXN-9 is another HMX formulation with an initial density of 1.74 g/cc and composed of 92.8 wt% HMX, 5.3 wt% DOA, and 1.9 wt% Hytemp 4454. Three x-ray images viewed down the cylinder axis are shown on the left and the transmission integrated horizontally through the region of increased transmission with 2 mm vertical resolution is shown on the right, with frame time relative to triggering noted in the figure. The transmission images are normalized and each image is divided by a pre-ignition static to more easily highlight changes in transmission in this formulation. The solid black lines are again guides to the eye. We observe the same overall structure of ignition, propagation and consumption in the increased transmission apparent in the images and quantified in the integrated intensity. However, relative to PBX 9501 we observe a factor of approximately three decrease in the rate of radial propagation, with an edge velocity of 57 m/s. This is a fairly dramatic decrease in internal burn rate, although even lower rates

This manuscript was accepted by Appl. Phys. Lett. Click here to see the version of record.

of propagation have been observed in PBXN-9 by proton radiography with laser assisted ignition.[16] Another experiment on PBXN-9, viewed side on, is shown in Fig. 4. We see a similar result, with ignition beginning at the experiment center and propagating toward the boundary. The transmission integrated horizontally through the region of increased transmission with 2 mm vertical resolution is shown in the middle panel, and the transmission integrated vertically through the region of increased transmission with 2 mm horizontal resolution is shown in the rightmost panel, both for six frames with all frame times relative to triggering noted in the figure. The velocity obtained as in Fig. 3, is 58 m/s, similar to the radial propagation velocity.

The velocities observed in these experiments are expected to depend on the driving gaseous pressure generated by hot product gases. This pressure will be determined by the outflow condition established by the coupling of pressurization rate and flow out of the case in each experiment. These experiments are designed to be sealed to the relatively low gas phase pressurization during heating to ignition in order to provide a well controlled and predictable thermal ignition. Subsequent to ignition however the case midplane or other case penetrations will allow for flow of product gasses at much higher pressure out of the case. The resulting steady state pressure will then determine the combustion velocity.

These effects are illustrated in Fig. 5, where internal combustion subsequent to thermal ignition are shown. The sample is PBX 9502, which is 95% TATB and 5% Kel-f, encased in a single 1” long x ½” Al cylinder without a case midplane. There are two 1/32” circular penetrations of the case to allow the introduction of thermocouples at the internal sample midplane. Flow through these two apertures constitutes the only outflow

This manuscript was accepted by Appl. Phys. Lett. Click here to see the version of record.

condition on the internal combustion. Ten frames of a continuous x-ray movie obtained at 1 s integration and interframe time are shown in Fig. 5(a). The frames show a transmission ratio of the dynamic images divided by a pre-ignition static image, with lighter denoting higher transmission/lower density. Frames are shown every 3 seconds during a 30 s consumption by laminar conductive burning, with the initial frame shown at top left, proceeding to the right and then from left to right in the bottom row. The initial frame is shown at very high contrast to illustrate the weak ignition volume observed prior to ignition. This is highlighted in Fig. 5(b) as two horizontally integrated line profiles with a 1 mm vertical resolution. The flat profile is obtained approximately 40 s before ignition and the second is taken as $t = 0$ in the subsequent frame timing during burning. The ignition volume is clearly observed but of only modest image contrast, peaking at 0.6%. Ignition is shown as a very fast vertical crack and expanding spherical volume in the second frame of Fig. 5(a). The nine frames after t=0 are shown at the same image contrast. Beginning in the third frame a front propagates from the ignition volume to either end of the case as a front ahead of which the transmission is unchanged and behind which a nearly constant region of high transmission remains. This is shown by horizontal line profiles, integrated through the center of the case with a 2 mm vertical resolution, in Fig. 5(c). The leading edges in the transmission image are clear as the steps between the initial transmission ratio of 1 and a final and constant ratio of approximately 1.3. A transmission ratio of 1.3 corresponds to an Al case without the explosive sample, as measured by radiography of the empty case. The location of the leading edge in the full radiographic movie, including those plotted in Fig. 5(c) at 3 s internals is plotted as a function of frame time in Fig. 5(d). The propagation rate is initially an accelerating

This manuscript was accepted by Appl. Phys. Lett. Click here to see the version of record.

parabolic function from t=1 to~6.2 s with a velocity of $v = 1.06 + 0.21t^{0.16}$, with v in mm/s and t in s. After t=6.2 s the rate linearizes to a constant velocity of 0.35 mm/s.

The propagation of internal combustion in TATB, in this instance, is unlike that in the preceeding HMX formulations. The observation of constant transmission both before and after the passage of the burn front indicates a classic, laminar conductive burn in this material under these conditions. The effect of the outflow condition is clear, with the pressure dependent rate of combustion accelerating in the beginning, but linearizing at x = 1 mm. This is the location of the thermocouple penetrations, which provide the simple outflow condition in this experiment and results in a constant velocity, and presumably driving pressure, after the front passes.

The overall mechanism of deflagration in these experiments appears to be a combination of classic conductive and convective combustion for the HMX based materials, and conductive for TATB, driven by the product gas pressure. These data clearly show the onset of internal burning and the propagation rate of combustion, followed by the conductive consumption of solid in the HMX based materials. Ongoing studies are directed toward understanding both the initial and steady state pressurization that results from the coupling of deflagration to the confining case, and verifying that the dependence of both convective and conductive rates of combustion on pressure for this environment of internal, convergent combustion is the same as that measured in strand burner experiments for external, divergent combustion.

ACKNOWLEDGMENTS

The authors wish to acknowledge support from the Science Campaign and Surety Programs administered by Los Alamos National Laboratory and the Joint Munitions Program administered jointly by the Departments of Energy and Defense.

REFERENCES:

1. B. W. Asay, in *Shock Wave Science and Technology Reference Library*, edited by Y. Hori (Springer-Verlag, Berlin, 2009), Vol. 5, pp. 617.
2. A. I. Atwood, T. L. Boggs, P. O. Curran, T. P. Parr, D. M. Hanson-Parr, C. F. Price and J. Wiknich, Journal of Propulsion and Power **15** (6), 740-747 (1999).
3. T. L. Boggs, Prog Astronaut Aeronaut **90**, 121-175 (1984).
4. M. Herrmann, W. Engel and N. Eisenreich, Propellants, Explosives, Pyrotechnics **17** (4), 190-195 (1992).
5. N. Kubota, Journal of Propulsion and Power **15** (6), 759-762 (1999).
6. J. L. Maienschein, J. F. Wardell, M. R. DeHaven and C. K. Black, Propellants, Explosives, Pyrotechnics **29** (5), 287-295 (2004).
7. A. Zenin, Journal of Propulsion and Power **11** (4), 752-758 (1995).
8. L. Smilowitz, B. F. Henson, J. J. Romero, B. W. Asay, A. Saunders, F. E. Merrill, C. L. Morris, K. Kwiatkowski, G. Grim, F. Mariam, C. L. Schwartz, G. Hogan, P. Nedrow, M. M. Murray, T. N. Thompson, C. Espinoza, D. Lewis, J. Bainbridge, W. McNeil, P. Rightley and M. Marr-Lyon, Journal of Applied Physics **111** (10), 103515 (2012).
9. L. Smilowitz, B. F. Henson, J. J. Romero, B. W. Asay, A. Saunders, F. E. Merrill, C. L. Morris, K. Kwiatkowski, G. Grim, F. Mariam, C. L. Schwartz, G. Hogan, P. Nedrow, M. M. Murray, T. N. Thompson, C. Espinoza, D. Lewis, J. Bainbridge, W. McNeil, P. Rightley and M. Marr-Lyon, Journal of Applied Physics **111** (10), 103516 (2012).
10. J. W. Tringe, E. A. Glascoe, J. R. Kercher, T. M. Willey, H. K. Springer, D. W. Greenwood, J. D. Molitoris, L. Smilowitz, B. F. Henson and J. L. Maienschein, presented at the Fourteenth Symposium (International) on Detonation, Coeur d'Alene, ID, 2010 (unpublished).
11. J. W. Tringe, J. D. Molitoris, L. Smilowitz, J. R. Kercher, H. K. Springer, B. F. Henson, E. A. Glascoe, D. W. Greenwood, R. G. Garza, B. M. Wong, J. D. Batteux and J. L. Maienschein, AIP Conference Proceedings **1195**, 424-427 (2009).
12. L. B. Smilowitz, B. F. Henson, J. J. Romero and D. O. Oschwald, Applied Physics Letters **104** (2014).
13. L. Smilowitz, B. F. Henson, M. M. Sandstrom, B. W. Asay and J. Romero, Thirteenth Symposium (International) on Detonation, 1026-1034 (2006).
14. L. Smilowitz, B. F. Henson, J. J. Romero and D. M. Oschwald, Applied Physics Letters **104** (024107) (2014).
15. L. Smilowitz, B. F. Henson, J. J. Romero, B. W. Asay, C. L. Schwartz, A. Saunders, F. E. Merrill, C. L. Morris, K. Kwiatkowski, G. Hogan, P. Nedrow, M. M. Murray, T. N. Thompson, W. McNeil, P. Rightley, M. Marr-Lyon and C. pRad, Physical Review Letters **100** (22), 228301 (2008).
16. L. Smilowitz, B. F. Henson, J. J. Romero, B. W. Asay and P. Collaboration, AIP Conference Proceedings **1195**, 436-439 (2009).

[16]FIGURE CAPTIONS

FIGURE 1: A schematic of the assembled experiment. Two half cylinders are combined to form a 2:1 aspect ratio cylinder encased in Aluminum. The arrows depict imaging axes both along the cylinder axis and side on to the cylinder. Other experimental configurations include a continuous cylindrical case, similar to this schematic, but assembled without a midplane.

FIGURE 2: X-ray images viewed down the cylinder axis and plotted in direct transmission for PBX 9501. Three frames subsequent to a dynamic trigger are shown on the left, showing the initial ignition volume and subsequent emanation of burning from this volume. On the right the normalized integration of the transmission across the diameter is shown for several frames.

FIGURE 3: X-ray images viewed down the cylinder axis and plotted in normalized transmission for PBXN-9. As in Fig 2. three frames subsequent to a dynamic trigger are shown on the left and the normalized integration of the transmission across the diameter is shown for several frames on the right.

FIGURE 4: X-ray images viewed side on to the cylinder axis and plotted in normalized transmission for PBXN-9. Three frames subsequent to a dynamic trigger are shown on the left and the normalized integration of the transmission both along the cylinder axis (horizontal) and vertically through the ignition volume are shown for several frames on the right.

FIGURE 5: Normalized X- ray images and analysis of conductive burning in PBX 9502. Fig. 5(a) Ten frames taken from an x-ray movie illustrating the initial ignition volume and the emanation of a conductive burn front in both directions along the cylinder axis. Fig. 5(b) Integrated transmission intensity along the cylinder axis 40 s prior to ignition and for the first frame in Fig. 5(a), illustrated the formation of the ignition volume. Fig. 5(c) Integrated transmission intensity along the cylinder axis during conductive propagration across the case. Fig. 5(d) Position of the leading edge of the conductive front as a function of frame time from which both initial acceleration and steady state velocity are obtained.

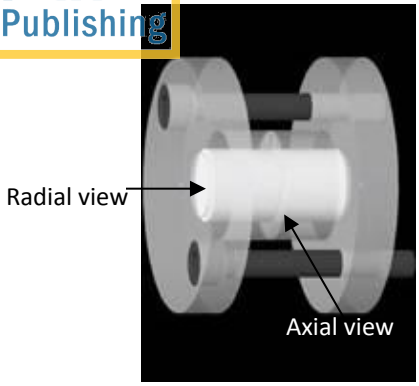

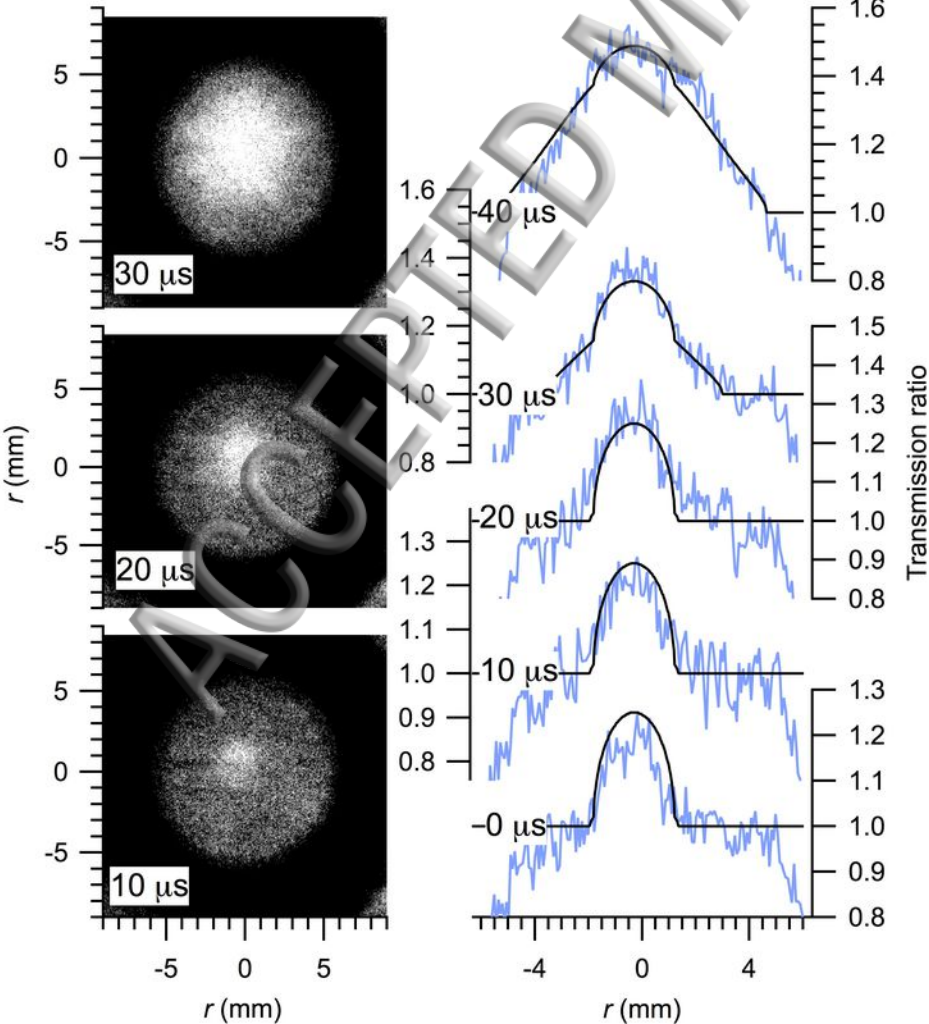
30 μs
20 μs
10 μs
r (mm)
r (mm)
-40 μs
-30 μs
-20 μs
-10 μs
-0 μs
Transmission ratio
r (mm)